



# CHORUS

This is the accepted manuscript made available via CHORUS. The article has been published as:

## Absence of Long-Range Order in a Triangular Spin System with Dipolar Interactions

Ahmet Keleş and Erhai Zhao

Phys. Rev. Lett. **120**, 187202 — Published 3 May 2018

DOI: [10.1103/PhysRevLett.120.187202](https://doi.org/10.1103/PhysRevLett.120.187202)

# Absence of long-range order in a triangular spin system with dipolar interactions

Ahmet Keleş<sup>1,2</sup> and Erhai Zhao<sup>2</sup>

<sup>1</sup>*Department of Physics and Astronomy, University of Pittsburgh, Pittsburgh, Pennsylvania 15260, USA*

<sup>2</sup>*Department of Physics and Astronomy, George Mason University, Fairfax, Virginia 22030, USA*

Antiferromagnetic Heisenberg model on the triangular lattice is perhaps the best known example of frustrated magnets, but it orders at low temperatures. Recent density matrix renormalization group (DMRG) calculations find that next nearest neighbor interaction  $J_2$  enhances the frustration and leads to a spin liquid for  $J_2/J_1 \in (0.08, 0.15)$ . In addition, DMRG study of a dipolar Heisenberg model with longer range interactions gives evidence for a spin liquid at small dipole tilting angle  $\theta \in [0, 10^\circ)$ . In both cases, the putative spin liquid region appears to be small. Here, we show that for the triangular lattice dipolar Heisenberg model, a robust quantum paramagnetic phase exists in a surprisingly wide region,  $\theta \in [0, 54^\circ)$ , for dipoles tilted along the lattice diagonal direction. We obtain the phase diagram of the model by functional renormalization group (RG) which treats all magnetic instabilities on equal footing. The quantum paramagnetic phase is characterized by a smooth continuous flow of vertex functions and spin susceptibility down to the lowest RG scale, in contrast to the apparent breakdown of RG flow in phases with stripe or spiral order. Our finding points to a promising direction to search for quantum spin liquids in ultracold dipolar molecules.

Quantum spin liquids evade conventional long-range order or symmetry breaking down to zero temperature [1–4]. These highly entangled states have unique properties including possible topological order or fractional excitations. Theoretically, the existence of certain spin liquid states is firmly established from exactly solvable models [5, 6]. While powerful numerical methods such as Density Matrix Renormalization Group (DMRG) and tensor networks (TN) have yielded clear evidence for spin liquids in geometrically frustrated spin models including the kagome lattice spin 1/2 Heisenberg model [7, 8] and the triangular lattice  $J_1$ - $J_2$  Heisenberg model [9, 10], the very nature of these spin liquids remains controversial. Experimentally, two class of materials, herbertsmithite [11] with kagome lattice structure and triangular lattice organic compounds [12–14], have emerged as strong candidates for quantum spin liquids. In the continuing search for spin liquids, it is useful to examine other model spin systems that are experimentally accessible.

A new class of quantum spin models, dubbed dipolar Heisenberg model, with long-range exchange interactions were recently predicted to harbor spin liquids. This model can be realized using polar molecules confined in deep optical lattices [15–18]. Similar spin models with tunable range and anisotropy have also been experimentally demonstrated with cold atoms with large magnetic moments [19], Rydberg-dressed atoms [20, 21], and trapped ions [22, 23]. These experiments thus motivate the exploration of the phase diagrams of dipolar Heisenberg model. Compared to the  $J_1$ - $J_2$  model, further range exchanges compete and sometimes enhance frustration. For example, TN calculation shows a narrow region of paramagnetic phase on the square lattice [24] which is also supported by RG analysis [25]. In Ref. 18, DMRG predicts a spin liquid phase on the triangular lattice for  $\theta$  between 0 to 10 degrees, where the dipole tilting angle  $\theta$  controls the spatial anisotropy of the exchange. The spin

liquid regions however seem small for both lattices. In addition, both DMRG and TN are limited to small lattice sizes: the range of interaction has to be truncated, and a small cluster is insufficient to accommodate the spiral order which has incommensurate wave vector and occupies much of the classical phase diagram. An independent, alternative approach is needed.

In this paper, we provide compelling evidence that the spin liquid region of the dipolar Heisenberg model can be expanded by five fold, to  $\theta \in [0, 54^\circ)$ , by tilting the dipoles towards the diagonal of the triangular lattice. Our idea exploits the tunable anisotropy available in experiments to suppress the stripe phase to arrive at a simple phase diagram which contains the quantum paramagnetic phase and the spiral phase, see Fig. 1(d). We argue that quantum paramagnetic phase is a spin liquid by comparing to DMRG. We further obtain the full phase diagram for arbitrary dipole tilting (Fig. 2) using numerical functional renormalization group which is capable of handling long-range interactions and spiral order using large cutoffs for the interaction range.

*Dipolar Heisenberg model and its classical phases.* Consider dipolar molecules localized in a deep optical lattice. Two rotational states of the molecule can be isolated to play the role of pseudospin 1/2. The dipole-dipole interaction induces long-range exchange interactions of the Heisenberg form (see Ref. [17, 18, 24] for details)

$$H = \sum_{i \neq j} J_{ij} \mathbf{S}_i \cdot \mathbf{S}_j, \quad (1)$$

where the sum is over all pairs of sites in a triangular lattice and  $\mathbf{S}_i = (S_i^x, S_i^y, S_i^z)$  are spin half operators at site  $i$ . We assume one molecule per site and all the dipole moments oriented along a common direction  $\hat{d}$  set by an external electric field. In terms of the polar angle  $\theta$  and the azimuthal angle  $\phi$  as shown in Fig. 1(a),  $\hat{d} = (\sin \theta \cos \phi, \sin \theta \sin \phi, \cos \theta)$ . The exchange interac-

tion then takes the dipolar form

$$J_{ij} = J_0[1 - 3(\hat{r}_{ij} \cdot \hat{d})^2]/r_{ij}^3 \quad (2)$$

where  $\mathbf{r}_{ij} = \mathbf{r}_i - \mathbf{r}_j$  for spins at sites  $\mathbf{r}_i$  and  $\mathbf{r}_j$ . Here the lattice constant is taken to be unity and the energy unit is given by  $J_0$ , the leading dipolar exchange.

The dipolar Heisenberg model, Eq. (1)-(2), is severely frustrated. In addition to the lattice geometric frustration, various (the nearest, second and further neighbor) exchanges, with their relative magnitude and sign controlled by dipole tilting [Fig. 1(c)], prefer different, competing long-range orders. To appreciate the possible orders, we first solve this model for classical spins [26]. Consider for example the case of  $\phi = 0$ , i.e.  $\hat{d}$  tilting along the  $x$ -axis, and varying  $\theta$ . From  $\theta = 0^\circ$  to  $\sim 20^\circ$ , it has the familiar  $120^\circ$  order. Stripe order takes over for  $\theta \in (20^\circ, 60^\circ)$ , with the spins aligned along  $x$  but alternating ( $\mathbf{S} \rightarrow -\mathbf{S}$ ) along  $y$ . For all other  $\theta$  values, the classical ground state is a spiral with incommensurate wave vector  $\mathbf{q}(\theta, \phi)$ . As  $\phi$  is increased, the stripe phase shrinks and eventually vanishes. It is largely dictated by symmetry: stripes along the lattice direction would break the reflection symmetry of the Hamiltonian with respect to the  $\hat{z} - \hat{d}$  plane and cost energy. This trend will continue to hold in the quantum phase diagram. The energy minima of the spiral and  $120^\circ$  phase are very shallow, a symptom of frustration [26]. As we will show below, they are easily melted by quantum fluctuations, leading to a drastically reconstructed phase diagram, Fig. 1(d).

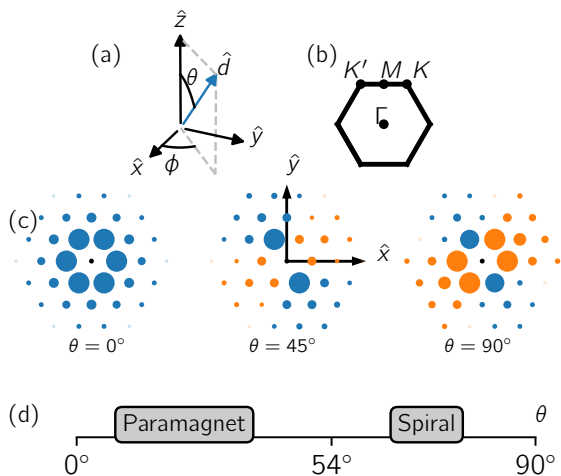


FIG. 1. (Color online) Dipolar Heisenberg model on the triangular lattice in the  $xy$  plane. (a) The exchange  $J_{ij}$  depends on the dipole orientation  $\hat{d}$ , with polar angle  $\theta$  and azimuthal angle  $\phi$ . (b) High symmetry points within the Brillouin zone. (c) The competing exchange couplings  $J_{ij}$  (site  $i$  is at the origin) for  $\phi = 30^\circ$  and  $\theta = 0^\circ, 45^\circ$  and  $90^\circ$  respectively. The size of the circle indicates the magnitude of  $J_{ij}$ , with positive (negative)  $J_{ij}$  shown in blue (orange). (d) The zero temperature phase diagram at  $\phi = 30^\circ$  includes a wide quantum paramagnetic phase,  $\theta \in [0, 54^\circ)$ , and a spiral phase.

*Pseudo-fermion FRG.* The key to find the phase diagram of the quantum dipolar Heisenberg model is an accurate, unbiased many-body technique that can treat the spiral order, long-range interactions, and large lattices. Functional renormalization group (FRG) is well suited for this purpose. It starts with the bare interaction, and systematically integrates out the high energy, short wave length fluctuations to track the flow of the effective action functional. Under the flow toward lower energy and longer wave length, the leading many-body instability emerges as the dominant divergence. We follow the pseudo-fermion FRG (pf-FRG) put forward by Reuther and Wölfle, which has been extensively benchmarked against other methods and applied to frustrated spin models [27–34]. The spin model Eq. (1) is first rewritten in a fermionic representation via  $\mathbf{S}_i = \frac{1}{2}\sigma_{\alpha\beta}\psi_{\alpha i}^\dagger\psi_{\beta i}$  where  $\psi$ 's are fermionic field operators. The resulting interacting fermion problem is then solved using the well-established fermionic FRG developed for strongly correlated electrons [35–38]. Specifically, vertex expansion up to one loop order yields the flow equations for the fermion self energy  $\Sigma$  and the effective interaction vertex  $\Gamma$  as functions of the sliding RG scale  $\Lambda$ ,

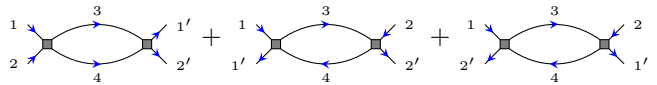
$$\partial_\Lambda \Sigma(\omega_1) = - \sum_2 \Gamma_{1,2;1,2} S(\omega_2), \quad (3)$$

$$\partial_\Lambda \Gamma_{1',2';1,2} = \sum_{3,4} \Pi(\omega_3, \omega_4) \left[ \frac{1}{2} \Gamma_{1',2';3,4} \Gamma_{3,4;1,2} - \Gamma_{1',4;1,3} \Gamma_{3,2';4,2} + \Gamma_{2',4;1,3} \Gamma_{3,1';4,2} \right]. \quad (4)$$

Hereafter the  $\Lambda$  dependence of  $\Sigma$ ,  $\Gamma$ ,  $G$ ,  $S$  etc. is omitted for brevity, and we use the shorthand notation  $\Gamma_{1',2';1,2} \equiv \Gamma(i_1, \alpha_1, \omega_1, i_2, \alpha_2, \omega_2; i'_1, \alpha'_1, \omega'_1, i'_2, \alpha'_2, \omega'_2)$  with site index  $i$ , spin  $\alpha$  and frequency  $\omega$ . The sum denotes integration over  $\omega$  as well as summation over lattice sites and spin. The scale-dependent propagators are defined by

$$G(\omega) = \frac{\Theta(|\omega| - \Lambda)}{i\omega + \Sigma(\omega)}, \quad S(\omega) = \frac{\delta(|\omega| - \Lambda)}{i\omega + \Sigma(\omega)}. \quad (5)$$

Note that the bare fermion propagator only has frequency dependence,  $G^{(0)}(\omega) = 1/i\omega$  [39]. Eq. (4) includes the particle-particle, the particle-hole as well as the exchange channel as shown by the following diagrams:



We adopt an improved truncation scheme beyond one loop [40] where the bubble  $\Pi$  is given by the full derivative

$$\Pi(\omega_3, \omega_4) = - \frac{d}{d\Lambda} [G(\omega_3)G(\omega_4)]. \quad (6)$$

The first order nonlinear integro-differential equations in Eq. (3) and (4) are supplemented by the following initial

conditions at the ultraviolet scale  $\Lambda_{UV} \rightarrow \infty$ ,

$$\begin{aligned} \Sigma(\omega)|_{\Lambda_{UV}} &= 0, \\ \Gamma_{1,2;1',2'}|_{\Lambda_{UV}} &= \frac{1}{4} \sigma_{\alpha_1 \alpha'_1}^\mu \sigma_{\alpha_2 \alpha'_2}^\mu J_{i_1, i_2} \delta_{i_1 i'_1} \delta_{i_2 i'_2} - (1' \leftrightarrow 2'). \end{aligned} \quad (7)$$

We numerically solve the coupled flow equations Eq. (3)-(4) together with the initial condition Eq. (7) and the dipolar exchange Eq. (2) using the fourth order Runge-Kutta, for a logarithmic frequency grid of  $N_\omega$  frequencies, by taking  $N_\Lambda$  RG steps from bare scale  $\Lambda_{UV}$  down to zero. We keep all couplings  $\Gamma$  within an  $N_L \times N_L$  parallelogram on the triangular lattice [26]. The computational cost scales with  $N_\Lambda \cdot N_L^2 \cdot N_\omega^4$ . We perform simulations up to  $N_L = 13$ ,  $N_\omega = 64$ , and  $N_\Lambda = 4N_\omega$ , i.e. four RG steps between two neighboring frequency points. Following the efficient spin and frequency parametrization scheme of Ref. 27, and exploiting the reflection symmetry of  $H$ , we still end up with over 22 million coupling constants ( $\Gamma$ s). To make the calculation tractable, the FRG code is designed to run parallel on thousands of graphic processing units. We have benchmarked it and found good agreement with known FRG results on the square [27] and triangular [34] lattice  $J_1$ - $J_2$  model.

From  $\Gamma$  and  $\Sigma$ , we compute the static spin-spin correlation functions in real space and then Fourier transform to obtain the spin susceptibility  $\chi(\mathbf{p})$  [27]. Let  $\chi_{\max}$  be the maximum value of  $\chi$  reached at wave vector  $\mathbf{p} = \mathbf{p}_{\max}$  within the Brillouin zone shown in Fig. 1(b). Together  $\chi(\mathbf{p})$  and  $\mathbf{p}_{\max}$  offer clues about the onset or lack of long-range order under the FRG flow. Typically  $\chi_{\max}$  displays Curie-Weiss behavior for  $\Lambda \gg 1$  until the build-up of quantum correlations starts to kick in around  $\Lambda \sim 1$ . An instability towards long range order is signaled by the divergence of  $\chi_{\max}$  at some critical scale  $\Lambda_c < 1$ . The finite cluster size and the truncation and discretization regularize the divergence, and replace it with unstable, irregular and oscillatory flow below  $\Lambda_c$ . Despite this, the breakdown of the smooth flow is unmistakable, and the type of incipient order can be inferred from the location of  $\mathbf{p}_{\max}$ . It may also happen that the flow of  $\chi$  remains stable and smooth down to the lowest RG scale  $\Lambda \rightarrow 0$ . Then the system settles into a paramagnetic phase.

To orient the full FRG solution and compare with the classical results, we first carry out static FRG, i.e. solving the flow equations by ignoring all  $\omega$  dependences [26, 41]. This approximation was shown to be consistent with random phase approximation and Luttinger-Tisza method [41]. From the flow of  $\Gamma$ , we extract a ‘‘critical scale’’  $\Lambda_s$ , at which the maximum value of  $\Gamma$  reaches a large cutoff value (diverges). Thus  $\Lambda_s$  serves as a rough estimation of the critical temperature for the long-range order. Fig. 2 shows the resulting  $\Lambda_s$  in false color with contour lines. Here we find good agreement with the classical analysis. The 120° order, where  $\chi$  shows maxima at the corners of the Brillouin zone, lies at small  $\theta$ . For increasing  $\theta$ , peaks at  $K$  and  $K'$  come together and merge at the  $M$  point,

indicating the stripe phase. For even larger  $\theta$ , the peak at  $M$  moves towards the  $\Gamma$  point, signaling the spiral order. Fig. 2 also shows that the spiral phase has the largest  $\Lambda_s$  (in green) whereas  $\Lambda_s$  is significantly suppressed (in dark blue) in the region around  $\theta \sim 15^\circ$  and near the phase boundaries. These dark areas are where spin liquid is suspected to reside.

*Phase diagram from pf-FRG.* Solving the flow equations with full frequency dependence along multiple cuts on the  $(\theta, \phi)$  plane and examining the flow of  $\chi_{\max}$  and the profile of  $\chi(\mathbf{p})$  in momentum space, we arrive at the zero temperature phase diagram of the dipolar Heisenberg model on triangular lattice shown in Fig. 2. The solid line and the dashed line mark the phase boundary between three major phases: the stripe, the spiral, and the quantum paramagnetic (PM) phase. The most striking result from pf-FRG is *the abundance of the PM phase*. A large portion of the classical spiral, including the 120° order, completely melts due to strong quantum fluctuations and gives way to quantum paramagnet. Compared to the  $J_1$ - $J_2$  Heisenberg model which shows a narrow region of spin liquid between the 120° and stripe order [9, 10], here the long-range dipolar exchanges suppress the 120° order to favor a disordered state. Our result agrees with earlier DMRG study of dipolar Heisenberg model for  $\phi = 0$  with truncated interactions [18]. Both predict a spin disordered phase for  $\theta < \theta_c$ , with  $\theta_c \sim 19^\circ$  from pf-FRG and  $\theta_c \sim 10^\circ$  from DMRG. Our new insight is that the PM phase becomes much broader,  $\theta_c \sim 54^\circ$ , if we tune  $\phi$  to  $30^\circ$  to suppress the stripe phase.

Now we discuss the pf-FRG results for a few representative points on the phase diagram. Let us start with the point  $\mathcal{P}_1$  in Fig. 2,  $\theta = 10^\circ$ ,  $\phi = 5^\circ$ . The spin susceptibility profile  $\chi(\mathbf{p})$  at  $\Lambda \approx 0.2$  is shown in the middle panel. It peaks at  $K$  and  $K'$ , indicating the 120° correlations. There is however no long-range order. We find instead a remarkably smooth flow of  $\chi_{\max}$  down to  $\Lambda \rightarrow 0$  without any sign of instability in the bottom panel of Fig. 2. Note that small fluctuations at small  $\Lambda$  are artifacts due to the frequency discretization and they diminish with finer grid. Similar PM behaviors are observed for point  $\mathcal{P}_2$  and  $\mathcal{P}_3$  at larger values of  $\phi$ , with the  $\chi(\mathbf{p})$  profile titled accordingly. These are our most significant findings.

Moving from point  $\mathcal{P}_1$  towards  $\mathcal{M}_1$ , the peaks at  $K$  and  $K'$  first become flatter and eventually coalesce at  $\theta = 17^\circ$ . Here  $\chi_{\max}$  shows a massive degeneracy in  $\mathbf{p}$ -space: it peaks along the entire  $K$ - $K'$  line. Beyond this point, the flow of  $\chi_{\max}$  shows increasing jumps at small  $\Lambda$ , and a kink (or turning point, indicated by the small arrow) is developed for  $\theta > 19^\circ$ . At the point  $\mathcal{M}_1$ ,  $\chi(\mathbf{p})$  is sharply peaked at  $M$ , and the flow becomes unstable at small  $\Lambda$ , clearly indicating the stripe phase. Increasing  $\theta$  further beyond the point  $\mathcal{M}_2$ ,  $\chi(\mathbf{p})$  develops a peak at a location between the  $M$  and  $\Gamma$  point. Similar result is obtained for other values of  $\phi$ , such as the  $\mathcal{M}_3$  point in Fig. 2. Here, the sharp peak of  $\chi(\mathbf{p})$  as well as the

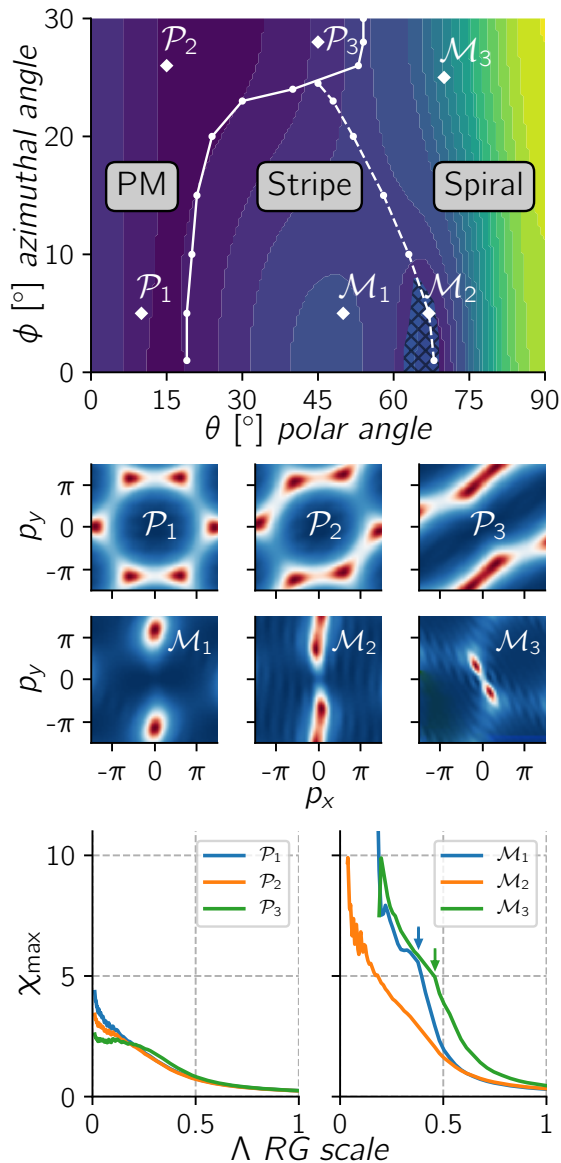


FIG. 2. (Color online) Zero temperature phase diagram of the dipolar Heisenberg model on triangular lattice as a function of the dipole tilting angle  $(\theta, \phi)$  showing the quantum paramagnetic (PM), stripe and spiral phases. Solid and dashed white lines are the phase boundaries (see main text). Color contours shows estimated critical temperature  $\Lambda_s$  from static FRG. Spin susceptibility profiles  $\chi(\mathbf{p})$  at scale  $\Lambda < 0.5$  are shown in the middle panels for representative points marked with  $\mathcal{P}_1$ ,  $\mathcal{M}_1$  etc.. The flows of peak susceptibility  $\chi_{\max}$  are shown in the bottom panels. For  $\mathcal{M}_1$  and  $\mathcal{M}_3$ , the flow becomes unstable below some RG scale indicated by the arrows.

unstable flow unambiguously identify the spiral order.

To locate the phase boundaries in a systematic manner, we introduce an empirical measure to quantify and detect the breakdown of smooth FRG flow. For a given dipolar tilting, we compute  $f(\theta, \phi) = \sum_{\Lambda} (\chi_{\max}|_{\Lambda} - \chi_{\max}|_{\Lambda-d\Lambda})^2$ , i.e. the “sum of unphysical jumps” during the flow. The

value of  $f$  is very small in the paramagnetic phase because of smooth continuous flow, and very large for ordered phases because their unstable flow [26]. By comparing to DMRG, we know that at  $\theta = 0$ , independent of  $\phi$ , the system is deep inside the PM phase. Thus, it provides a standard measure  $f_0 = f(\theta = 0, \phi = 0)$ . If  $f(\theta, \phi) \leq f_0$ , the low energy flow is equally smooth or even smoother than that at  $\theta = 0$ , we then conclude the system flows to a disordered, paramagnetic phase. The resulting boundary of the PM phase is shown by the solid white line bending to the right in Fig. 2. The transition from PM to stripe is marked by a rapid increase in  $f/f_0$ . In contrast, the transition from stripe to spiral is signaled by smoothing of the flow and thus suppression of  $f$  (see the flow for  $\mathcal{M}_2$  in Fig. 2). We identify the stripe-spiral boundary as where  $f$  develops a local minimum along the horizontal cuts in the  $(\theta, \phi)$  plane. It is shown by the white dashed line bending to the left in Fig. 2. This line is also where the peaks in  $\chi(\mathbf{p})$  become smeared and the location of  $\mathbf{p}_{\max}$  begins to change character. In the hatched region around  $\mathcal{M}_2$  in Fig. 2, the flow is much smoother than  $\mathcal{M}_1$  and  $\mathcal{M}_3$  at small  $\Lambda$ . It is analogous to  $\mathcal{P}_1$  but  $\chi_{\max}$  reaches a much bigger value at  $\Lambda = 0$ . Therefore, this small region is likely a second PM phase, but on the verge of being ordered.

To summarize, our numerical FRG calculation reveals a quantum paramagnetic phase occupying a large portion of the phase diagram of the dipolar Heisenberg model. FRG enables us to reach large cutoff distances for an accurate description of the dipolar exchange and the spiral order. It describes quantum fluctuations beyond the spin-wave or Schwinger-boson theory. The widespread lack of divergence in  $\chi$  is unexpected. In hindsight, three factors conspire to suppress long-range order. First is the lattice geometric frustration, stemming from the long-range dipolar exchange (see Fig. 1). Even in the  $J_1$ - $J_2$  model, finite  $J_2$  enhances paramagnetic behavior [9, 10, 42]. Longer range exchanges lead to very flat classical energy landscape, with distinct orders close in energy. These weak classical orders are melted by quantum fluctuations to form a quantum paramagnet.

Our results suggest that experiments on ultracold quantum gases of polar molecules with electric dipole moments or atoms with large magnetic dipole moments are promising systems to explore frustrated magnetism and search for spin liquids [15, 19]. There are two limitations to the current pf-FRG method. First, the flow equation is restricted to one-loop diagrams. An improvement is to include two-loop terms as achieved recently in Ref. [43]. Second, current pf-FRG implementation cannot directly characterize the spin liquid states. Future work is needed to elucidate the nature of the predicted spin

liquid states in various spin 1/2 models on the triangular lattice [44, 45], which remains an outstanding open problem.

This work is supported by NSF Grant No. PHY-1707484 and AFOSR Grant No. FA9550-16-1-0006. A.K. is also supported by ARO Grant No. W911NF-11-1-0230. The GPU used for the calculation is provided in part by the NVIDIA Corporation.

- 
- [1] L. Balents, *Nature* **464**, 199 (2010).
- [2] P. A. Lee, *J. Phys.: Conf. Ser.*, **529**, 012001 (2014).
- [3] L. Savary and L. Balents, *Rep. Prog. Phys.* **80**, 016502 (2016).
- [4] Y. Zhou, K. Kanoda, and T.-K. Ng, *Rev. Mod. Phys.* **89**, 025003 (2017).
- [5] A. Y. Kitaev, *Annals of Physics* **303**, 2 (2003).
- [6] A. Y. Kitaev, *Annals of Physics* **321**, 2 (2006).
- [7] S. Yan, D. A. Huse, and S. R. White, *Science* **332**, 1173 (2011).
- [8] S. Depenbrock, I. P. McCulloch, and U. Schollwöck, *Phys. Rev. Lett.* **109**, 067201 (2012).
- [9] Z. Zhu and S. R. White, *Phys. Rev. B* **92**, 041105 (2015).
- [10] W.-J. Hu, S.-S. Gong, W. Zhu, and D. N. Sheng, *Phys. Rev. B* **92**, 140403 (2015).
- [11] M. P. Shores, E. A. Nytko, B. M. Bartlett, and D. G. Nocera, *J. Am. Chem. Soc.* **127**, 13462 (2005).
- [12] Y. Shimizu, K. Miyagawa, K. Kanoda, M. Maesato, and G. Saito, *Phys. Rev. Lett.* **91**, 107001 (2003).
- [13] Y. Kurosaki, Y. Shimizu, K. Miyagawa, K. Kanoda, and G. Saito, *Phys. Rev. Lett.* **95**, 177001 (2005).
- [14] M. Yamashita, N. Nakata, Y. Senshu, M. Nagata, H. M. Yamamoto, R. Kato, T. Shibauchi, and Y. Matsuda, *Science* **328**, 1246 (2010).
- [15] B. Yan, S. A. Moses, B. Gadway, J. P. Covey, K. R. Hazzard, A. M. Rey, D. S. Jin, and J. Ye, *Nature* **501**, 521 (2013).
- [16] K. R. A. Hazzard, B. Gadway, M. Foss-Feig, B. Yan, S. A. Moses, J. P. Covey, N. Y. Yao, M. D. Lukin, J. Ye, D. S. Jin, and A. M. Rey, *Phys. Rev. Lett.* **113**, 195302 (2014).
- [17] A. V. Gorshkov, S. R. Manmana, G. Chen, E. Demler, M. D. Lukin, and A. M. Rey, *Phys. Rev. A* **84**, 033619 (2011).
- [18] N. Y. Yao, M. P. Zaletel, D. M. Stamper-Kurn, and A. Vishwanath, *Nature Physics* (2018), 10.1038/s41567-017-0030-7.
- [19] A. de Paz, A. Sharma, A. Chotia, E. Maréchal, J. H. Huckans, P. Pedri, L. Santos, O. Gorceix, L. Vernac, and B. Laburthe-Tolra, *Phys. Rev. Lett.* **111**, 185305 (2013).
- [20] P. Schauß, M. Cheneau, M. Endres, T. Fukuhara, S. Hild, A. Omran, T. Pohl, C. Gross, S. Kuhr, and I. Bloch, *Nature* **491**, 87 (2012).
- [21] H. Labuhn, D. Barredo, S. Ravets, S. De Léséleuc, T. Macrì, T. Lahaye, and A. Browaeys, *Nature* **534**, 667 (2016).
- [22] J. W. Britton, B. C. Sawyer, A. C. Keith, C.-C. J. Wang, J. K. Freericks, H. Uys, M. J. Biercuk, and J. J. Bollinger, *Nature* **484**, 489 (2012).
- [23] R. Islam, C. Senko, W. Campbell, S. Korenblit, J. Smith, A. Lee, E. Edwards, C.-C. Wang, J. Freericks, and C. Monroe, *Science* **340**, 583 (2013).
- [24] H. Zou, E. Zhao, and W. V. Liu, *Phys. Rev. Lett.* **119**, 050401 (2017).
- [25] A. Keles and E. Zhao, *arXiv:1803.02904* (2018).
- [26] See online Supplementary Materials, which include Refs. 46 and 47.
- [27] J. Reuther and P. Wölfle, *Phys. Rev. B* **81**, 144410 (2010).
- [28] J. Reuther and R. Thomale, *Phys. Rev. B* **83**, 024402 (2011).
- [29] J. Reuther, D. A. Abanin, and R. Thomale, *Phys. Rev. B* **84**, 1 (2011).
- [30] J. Reuther, R. Thomale, and S. Rachel, *Phys. Rev. B* **90**, 1 (2014).
- [31] R. Suttner, C. Platt, J. Reuther, and R. Thomale, *Phys. Rev. B* **89**, 020408 (2014).
- [32] F. L. Buessen and S. Trebst, *Phys. Rev. B* **94**, 235138 (2016).
- [33] Y. Iqbal, H. O. Jeschke, J. Reuther, R. Valentí, I. I. Mazin, M. Greiter, and R. Thomale, *Phys. Rev. B* **92**, 220404 (2015).
- [34] Y. Iqbal, W.-J. Hu, R. Thomale, D. Poilblanc, and F. Becca, *Phys. Rev. B* **93**, 144411 (2016).
- [35] W. Metzner, M. Salmhofer, C. Honerkamp, V. Meden, and K. Schönhammer, *Rev. Mod. Phys.* **84**, 299 (2012).
- [36] P. Kopietz, L. Bartosch, and F. Schütz, *Introduction to the Functional Renormalization Group*, Lecture Notes in Physics, Vol. 798 (Springer, Berlin, Heidelberg, 2010).
- [37] S. Bhongale, L. Mathey, S.-W. Tsai, C. W. Clark, and E. Zhao, *Phys. Rev. Lett.* **108**, 145301 (2012).
- [38] A. Keleş and E. Zhao, *Phys. Rev. A* **94**, 033616 (2016).
- [39] The chemical potential is set to zero to enforce the fermion number constraint, see Ref. [27].
- [40] A. A. Katanin, *Phys. Rev. B* **70**, 115109 (2004).
- [41] M. L. Baez and J. Reuther, *Phys. Rev. B* **96**, 045144 (2017).
- [42] S. N. Saadatmand and I. P. McCulloch, *Phys. Rev. B* **96**, 075117 (2017).
- [43] M. Rueck and J. Reuther, *arXiv:1712.02535* (2017).
- [44] A. M. Essin and M. Hermele, *Phys. Rev. B* **87**, 104406 (2013).
- [45] Y.-M. Lu, *Phys. Rev. B* **93**, 165113 (2016).
- [46] F. L. Buessen, M. Hering, J. Reuther, and S. Trebst, *Phys. Rev. Lett.* **120**, 057201 (2018).
- [47] S. Göttel, S. Andergassen, C. Honerkamp, D. Schuricht, and S. Wessel, *Phys. Rev. B* **85**, 214406 (2012).